Peer reviewed version

Link to published version (if available):
10.1016/j.cub.2018.09.054

Link to publication record in Explore Bristol Research
PDF-document

University of Bristol - Explore Bristol Research
General rights

Title: Abnormal locus coeruleus activity during sleep
alters sleep signatures of memory consolidation
and impairs place cell stability and spatial memory

Kevin M. Swift[1], Brooks A. Gross[2], Michelle Frazer[2], David S. Bauer[1], Kyle Clark[1], Elena Vazey[3], Gary Aston-Jones[3], Yong Li[4], Anthony E. Pickering[4], Susan Sara[5,6], Gina R. Poe[1,2,7,*]

[1]Department of Molecular and Integrative Physiology, University of Michigan, Ann Arbor, MI 48109, USA
[2] Neuroscience Department, University of California Los Angeles, Los Angeles, CA 90095, USA
[3]Brain Health Institute, Rutgers University, New Brunswick, NJ 08854, USA
[4]School of Physiology, Pharmacology & Neuroscience, University of Bristol, Bristol, UK BS8 1TD
[5]Center for Interdisciplinary Research in Biology, College de France, Paris, France 75005
[6]Child and Adolescent Psychiatry, New York University Medical School, New York, NY 10003, USA
[7]Lead Contact
*Corresponding Author: ginapoe@ucla.edu
Keywords: sleep, locus coeruleus, hippocampus, spindle

Summary

Sleep is critical for proper memory consolidation. The locus coeruleus (LC) releases norepinephrine throughout the brain except when the LC falls silent throughout rapid eye movement (REM) sleep and prior to each sleep spindle during NREM sleep. We hypothesize that these transient LC silences allow the synaptic plasticity necessary to incorporate new information into preexisting memory circuits. We found that spontaneous LC activity within sleep spindles in the rat triggers a decrease in spindle power. By optogenetically stimulating norepinephrine-containing LC neurons during sleep at 2 Hz, we reduced CA1 NREM spindle occurrence, as well as NREM delta power and REM theta power without causing arousals or changing sleep amounts. Stimulating the LC during sleep following a hippocampus-dependent food location learning task interfered with consolidation of newly learned locations, and reconsolidation of previous locations. The LC stimulation-induced reduction in sleep spindles and REM theta, and a reduced in ripple-spindle coupling all correlated with decreased hippocampus-dependent performance on the reversal task. Thus periods of LC silence during sleep following learning are essential for normal spindle generation and consolidation of spatial memories.

Introduction

Much work has focused on the interplay between the hippocampus and neocortex during sleep to promote memory [1–4]. However, the neuromodulatory systems necessary for memory formation during waking are relatively unexamined during sleep. The noradrenergic system and its source for the forebrain, the locus coeruleus (LC), is active during waking to promote vigilance, and is responsive to novel information, enabling rapid learning by boosting long term potentiation (LTP) mechanisms [5,6]. During sleep, decreased LC neuronal activity was thought to simply promote somnolence [7].

However, the decrease in LC firing is not uniform across all phases of sleep in rats and higher mammals [8–10]. The LC is active throughout the slow wave sleep stage of NREM sleep, but during rapid eye movement (REM) sleep, LC neurons fall silent while cholinergic activity increases [10] and 5-9 Hz theta frequency activity dominates in the electrographic signals. Additionally, LC neurons fall silent prior to the onset of each sleep spindle (10-15 Hz high amplitude oscillations in electrographic signals) in NREM, as compared to the rest of NREM sleep [10]. Both REM sleep theta and sleep spindles have been shown to be important for memory consolidation [11–14], but the physiological relevance of these LC silences for the function of sleep for memory has not been evaluated. We hypothesize that, because norepinephrine supports only strengthening of neuronal synapses (LTP) or neutral synaptic weight changes in memory circuits, these transient LC silences uniquely allow the depotentiation (resetting strengthened synapses to baseline efficacy) necessary for certain types of learning [15,16].

We tested whether these transient decreases in LC firing are necessary for the generation of normal REM sleep theta and NREM sleep spindles as well as for memory consolidation and next day memory neural encoding. Using optogenetics to maintain waking LC activity levels during NREM and REM sleep combined with simultaneous tetrode recordings of hippocampal place cells during place learning, we tested the effect of increased LC activity during sleep on a sleep-dependent hippocampal place memory learning task [17]. Although the overall stability and duration of sleep states were not changed, the learning-related signatures of NREM and REM sleep were impaired. Results showed that LC silences are necessary for normal NREM sleep delta power, REM sleep theta power, normal sleep spindle generation and the coupling of sleep spindles to hippocampal ripples —drops in all of which correlated with decreases in different facets of task performance. Furthermore, while overall place cell firing rates were unchanged during sleep or wakefulness, sustained LC activity during sleep also led to decreased next day encoding stability of reward locations on the task.

Results

Endogenous LC activity decreases during spindle-rich intermediate sleep. Tetrode recording of endogenous LC neural activity across sleep and wakefulness showed highest activity during waking and was significantly lower activity during all stages of sleep: NREM-slow wave sleep, NREM-intermediate sleep, and REM sleep. (Figure S1). Within NREM sleep, LC neuron activity during spindle-rich intermediate sleep [18] was a similar to REM sleep. During REM sleep, LC activity reached its lowest point and was significantly reduced compared to waking. Our results show that both REM sleep and spindle-rich IS sleep are periods of greatly reduced LC neuronal activity.

Endogenous LC activity during sleep spindles terminates the spindle. Aston-Jones and Bloom [1981] demonstrated that LC neurons fire specifically in relation to sleep spindles: one second prior to the onset of sleep spindles, LC neurons are inactive, but during the spindle, these LC neurons resume firing (see example in Figure 1A). We posit that this resumption of LC activity leads to spindle termination, possibly through the depolarizing action of norepinephrine on

thalamocortical neurons whose hyperpolarization allows the voltage-gated Ca++ spikes that generate the sleep spindles [19,20]. We examined the timing of LC spikes occurring within spindles and outside of spindles and their respective relationship to spindle power (sigma band). We found that LC spikes within sleep spindles occurred when the spindles reached maximal sigma power and that LC spikes were followed by an immediate and rapid reduction of sigma power (Figure 1B, C). This phenomenon was spindle-specific as LC spikes occurring outside of sleep spindles (during NREM sleep) had no effect on sigma power.

LC optogenetic stimulation during sleep decreased NREM sleep spindle occurrence. Due to the precise timing of LC neuronal spikes during spindles, along with previous work showing that norepinephrine infusions into thalamic nuclei *in vitro* abolishes spindle generation [20], we hypothesized that optogenetically enhanced LC activity during sleep could be used to reduce spindle occurrence during NREM sleep. To test this, we expressed channelrhodopsin (ChR2) in LC cells under the control of PRSx8, a synthetic dopamine-beta hydroxylase promoter [21] (Figure S2A). Extracellular recordings of ChR2 expressing LC cells *in vivo,* showed light evoked action potentials in response to 473 nm light pulses (Figure S2B).

We conducted a series of experiments to determine what frequency of LC stimulation that was permissible to maintain sleep without evoking arousals (see methods and Figure S2C-E). We found 2 Hz LC stimulation did not generate arousals and further, was within normal physiological activity. Therefore 2 Hz was used throughout the remainder of the studies.

We then simulated ChR2+ rats at 2 Hz during sleep which resulted in a significant decrease in NREM sleep spindle occurrence compared to baseline sleep lacking stimulation in the same ChR2+ rats (Figure 1D).

LC stimulation during sleep impaired subsequent hippocampal spatial encoding. Sleep spindles are strongly implicated in memory consolidation and the integration of new information into existing knowledge [13,22]. Previous work from our lab showed that pharmacologically enhancing noradrenergic activity across the post-training sleep period (using the selective noradrenergic reuptake inhibitor Desipramine) impaired hippocampal learning [17]. In a separate cohort, we tested whether enhancing noradrenergic activity selectively during only post-training sleep through LC stimulation was sufficient to impair hippocampal spatial encoding. Rats were pretrained on a hippocampus-dependent spatial learning task [23] that presented food rewards at three familiar positions on an elevated octagonal track (Figure 2A). Once the rats reached behavioral criteria (< 1 error per lap) during the training period, they ran the track daily with food at the familiar task locations, and then ran the track for an additional 15 laps with two of the three food reward locations shifted to altered positions (the altered task) that remained in the same altered place for the last 15 laps each day. The function of the task was to evaluate whether rats could remember both reward location maps: the three previously consolidated, familiar locations and the new, altered locations. Following the familiar and altered track running session, we monitored rats' sleep-wake behavior via neck EMG and CA1 LFP activity, and optogenetically stimulated the LC at 2 Hz whenever the rat was asleep (both NREM and REM) in the 5-hour post learning period—which has been shown to be a critical period for hippocampal sleep dependent memory consolidation (see for review [24]). Stimulation occurred on the first two days as by 3 REM sleep signs of consolidation are already apparent [25,26].

We first examined the effect of LC stimulation on hippocampal place cell spatial encoding. Stimulating the LC during sleep after exposure on day 1 to both the familiar and the altered task resulted in reduced lap to lap spatial stability of place fields during both tasks on day 2 in ChR2+ rats (Figure 2B, E). Figure 2C and 2F show representative heat maps of place field locations across laps on both tasks with each fields associated stability metric (the Pearson correlation of the field firing maps across laps with higher r values representing higher spatial stability). The decrease in place field stability in ChR2+ rats went hand-in-hand with a significant increase in lap-to-lap shifts in place field location on both tasks (Figure 2D, G).

Next, we examined place field expansion. While performing a lap-based task, the center of mass (COM) of a place field (i.e. the region within the place field where the place cell has the highest activity) shows a net shift backwards across multiple laps, expanding the overall field size; i.e. the place cell fires slightly earlier on the track. This phenomenon is better known as place field backward expansion [27,28]. Place field backward expansion is a NMDA-dependent plasticity effect [29]. As place fields do not grow across days [30], the field size and place must reset between days and running sessions. We have previously posited that this reset function is accomplished by depotentiation driven by the absence of LC activity during REM sleep [25,26]. While place field backward expansion occurred normally on day 1 (before intervention) on both tasks, on day 2 in ChR2+ rats, the familiar place fields did not expand backwards, but rather, shifted abnormally forward (Figure S3B). There was also a significant increase in familiar task place field size on day 2 selectively in ChR2+ rats (Figure S3D). These abnormal expansion and forward shifts were not seen on the altered task (Figure S3A, C), suggesting a specific effect on previously consolidated-familiar spatial information.

Both spatial mapping abnormalities of place field stability, and abnormal place field backward expansion indicates that LC stimulation during sleep following learning on day 1 caused abnormal CA1 place field consolidation of the altered task and reconsolidation of the familiar task. Finally, these effects occurred independent of any changes in CA1 pyramidal firing rate during NREM, REM sleep, or waking (Two-way ANOVA, Sidak post hoc p=0.92, 0.66, and 0.98, respectively).

LC stimulation during post learning sleep impaired spatial learning and memory performance. Just as place encoding was impaired on both the altered and familiar task by enhanced LC activity during sleep, behavioral performance was similarly impaired on both tasks. On the altered task, ChR2+ rats showed no day-to-day improvement, whereas ChR2- rats improved significantly from day 1 to day 5 and performed significantly better than ChR2+ rats on day 4 and 5 (Figure 3A). Not surprisingly, given the place field encoding deficits, ChR2+ rats also performed significantly worse on the familiar task than ChR2- rats, showing a significant decline in performance between days 1 and 5, and performing worse than controls on day 4 and 5 (Figure 3B). To ensure that LC stimulation during sleep had no long-term effect on learning, both groups were run on a completely novel hippocampal task with new novel spatial cues and reward locations, followed by normal sleep each day. Both groups learned the novel task at similar rates and showed significant improvement in performance within two days (Figure 3C).

LC stimulation during sleep altered task solving strategies. In addition to the error count, we were curious to see whether rats utilized hippocampal strategies to solve the task or reverted to a random search strategy [31]. We termed errors "map errors" if they were errors committed at reward locations that differed between the tasks, and "procedural errors" if the error was at a location where the reward contingency remained static (i.e. checking any of the three box positions that were never rewarded or skipping the one box position that was rewarded on both tracks) (Figure 4A). For the altered task, as expected, ChR2- rats consistently committed significantly more map errors than procedural errors, checking for food in previously rewarded positions (Figure 4B). In contrast, in LC stimulated rats there was no difference in the number of map errors compared to procedural errors by day 2 and each day the average number of procedural errors climbed until they were on par with the number of map errors (Figure 4C)—suggesting adoption of a random search strategy. On the familiar task (after the first exposure to the altered maze on day 1), ChR2- rats committed significantly fewer procedural errors than map errors and showed an overall downward trend in procedural errors across days, whereas ChR2+ rats committed a similar number of procedural and map errors across days with an overall trend to increasing errors of both types across days (Figure 4D, E).

LC stimulation during sleep altered specific frequency bands, but not sleep architecture. We next examined whether LC sleep stimulation caused any change in sleep characteristics. Looking first at waking, there was no difference in the percent of the total time spent awake between ChR2- and ChR2+ rats, i.e. LC stimulation did not prevent sleep (Figure 5A). Within sleep, there was no difference in the percent of time spent in any state between groups (Figure 5B) and there was no difference in the number of transitions from either NREM sleep or REM sleep to waking (Figure 5C). That is, there was no increase in the number of arousals with LC stimulation. Finally, there was no rebound in sleep or change in percent spent in any sleep state on day 3 when no LC stimulation occurred.

However, LC sleep stimulation did cause decreases in CA1 spectral band power at several frequencies during specific sleep stages (Figure 5D, E). No change was seen in any band power during waking, although LC stimulation was turned off once signs of waking were observed. There was no LC-stimulation associated change in higher frequency bands such as slow gamma (30-50 Hz) or fast gamma (61-100 Hz) during any sleep state. However, both NREM slow wave sleep and NREM intermediate sleep showed a decrease in delta (1-4 Hz) band power during LC stimulation periods. These decreases in NREM-SWS delta power correlated with Day 5 procedural errors on both the familiar and altered task (Table S1). Intermediate sleep also decreased band power in the frequency range associated with sleep spindles: sigma (10-15 Hz). During REM sleep, LC stimulation decreased theta power (5-9 Hz) (Figure 6A) and the percent drop in theta power correlated with overall day 5 performance. Theta power suppression accompanied day 5 procedural errors (i.e. errors at boxes that did not change between mazes) on both familiar and altered maze tasks, but did not correlate with map errors (Table S1). Thus, NREM delta and REM sleep theta impairments corresponded with performance errors specifically in those areas of the maze that never changed their reward contingency. These types of errors can be associated with a general search pattern rather than reliance on a trusted map.

LC stimulation decreased sleep spindle occurrence.
In addition to frequency changes, we tested whether LC stimulation altered the rate of spindle occurrence during sleep following learning. While there was no difference in baseline spindle occurrence between groups (ChR2- 0.045±0.002

spindles/sec, ChR2+ 0.055±0.004 spindles/sec), the percent change from baseline to day 1 sleep was significant between groups: ChR2+ rats experienced a decrease in spindle occurrence and ChR2- animals saw an increase (Figure 6B). LC stimulation reduced spindle occurrence in rats performing our learning task as well as in rats without a learning task. However, the absence of a learning task significantly increased this reduction in spindle occurrence caused by LC stimulation (Figure S4). When LC optogenetic stimulation occurred within a spindle we found that spindle power decreased ~90 msec following light onset (Figure 6C). This 90 msec timeframe is consistent with the conduction of LC action potentials through unmyelinated axons to their terminals [32,33]. We found that the occurrence of spindles exceeding our inter-stimulus interval, i.e. spindles ≥0.6 seconds in length, were disproportionately reduced, whereas shorter spindles were unaffected (Figure 6D). This change in spindle occurrence from baseline to day 1 correlated with overall day 5 performance on the altered and familiar tasks. The change in spindle occurrence specifically correlated with day 5 map errors on the familiar task (i.e. box positions that changed between mazes), but not with procedural errors (Table S1).

Aberrant LC activity during sleep interfered with ripple-spindle coupling. Previous work has posited that the coupling of ripples to spindles is important for learning and memory consolidation [1,2]. Therefore, we examined whether LC stimulation had any effect on ripple-spindle coupling. During baseline sleep there was no difference between groups in ripple-spindle coupling, and coupling was significantly non-random in both groups when tested against shuffled data (Figure 7A). Yet, during day 1 sleep with LC stimulation, ChR2+ rats had significantly decreased coupling compared to ChR2- rats, although coupling was still nonrandom for both groups (Figure 7B). To ensure that this difference in coupling was not due to changes in CA1 ripple occurrence rate we analyzed ripples and found that there was no change in ripple occurrence or length between groups or across days (Figure S5B-E), and ripples did not correlate with behavioral performance (Table S1). Additionally, we examined ripple probability in relation to spindle onset and found that there was no difference between groups on either day (Figure S5F). Therefore, this change in ripple-spindle coupling was likely due to changes in spindles rather than ripples. Finally, the changes in coupling correlated with overall day 5 performance on the altered and familiar task, more specifically with both map errors and procedural errors on the familiar task and only procedural errors on the altered task (Table S1).

Discussion

Our present findings demonstrate that LC activity normally decreases during spindle-rich NREM-intermediate sleep as well as REM sleep. Endogenous LC activity during a sleep spindle leads to spindle termination, and optogenetically enhanced LC activity during sleep reduces spindle occurrence, as well as REM sleep theta power, while leaving sleep as a behavioral state intact. Further, LC stimulation during sleep following learning decreases the fidelity of hippocampal place encoding, while leaving hippocampal ripples and pyramidal cell activity unchanged. As a result, consolidation of spatial memory was also hampered, which led to rats utilizing non-hippocampal procedural strategies to solve the task. These alterations in learning strategies directly correlated with changes in sleep spindle occurrence and REM sleep theta power, which were the result of LC stimulation during sleep. We believe the normal drop in LC activity prior to each sleep spindle and during REM sleep—while not required to maintain somnolence—is important for normal NREM sleep spindle generation and REM sleep theta power, and, by extension, hippocampal memory consolidation [11,13].

Previous work has shown that the pressure for sleep spindles increases after learning and their increased occurrence correlates with memory consolidation [12,34,35]. Upregulation of sleep spindles improves memory [13,36]. We found that LC stimulation reduced the occurrence of sleep spindles more than 60%, while under the pressure of learning, LC stimulation significantly reduced spindles, but to a lesser magnitude, possibly due to a training-induced spindle drive. We provide here the first evidence that preventing an increase in sleep spindles following learning prevents consolidation of a new memory and reconsolidation of a familiar memory.

Persistent LC activity reduced REM sleep theta power, which could have REM sleep-dependent memory consolidation implications [25,37]. REM sleep is a time of synaptic downscaling [38]. Norepinephrine blocks depotentiation [6,39] and sleep-dependent synaptic downscaling [40]. Normally place fields maintain stable place coding over weeks [30], despite backwards expansion occurring during task performance [28], necessitating synaptic downscaling between sessions. We show that when we sustain LC activity across sleep, place fields grow abnormally large across days, providing indirect evidence of unchecked LTP and a failure to depotentiate during REM sleep. These REM sleep disruption results support Boyce et al., 2016 showing the importance of REM sleep theta for memory consolidation. We further provide indirect evidence of a possible depotentiation deficit underlying these consolidation errors.

In addition to decreasing sleep spindle occurrence and power, and REM sleep theta power, 2 Hz LC stimulation also led to a significant decrease in slow wave-delta power--which also correlated with the number of procedural errors on both tasks. Previous work in humans has highlighted the function of NREM slow waves in the consolidation of visual

perceptual and implicit paired-associate learning [41,43]. Artificial enhancement or disruption of slow waves has been shown to enhance paired-associate or impair motor skill memory consolidation, respectively [45,47]. In rodents LC neuron activity is shown to synchronize to the rising phase of slow waves [9]. It is possible that our manipulation of LC activity during sleep interferes with the timing of LC activity in relation to slow waves, which may result in decreased delta power or disrupt the effect of memory processing thought to occur during sharp-wave ripples at slow wave peaks. More work is necessary to understand the relationship between NREM slow waves and LC activity in relation to memory consolidation.

While previous work has highlighted the importance of noradrenergic activity in memory formation during waking [42,44,46,48], little has been done to examine what function the presence or, especially, the absence of norepinephrine during sleep may have on learning and memory. Further work is needed to understand if the effects of aberrant LC activity during sleep on hippocampal spatial encoding and memory are due to noradrenergic receptor activation or to dopamine, which is released from the same terminals when NE is depleted [49,50]. The low stimulation rate used in our study make dopaminergic mechanisms less likely.

An interesting facet of our results is the persistence of rodent behavioral performance deficits despite cessation of LC optogenetic stimulation. Although stimulation ceases after day 2, the ChR2+ rats' performance continues to decline. The initial decrease in performance up to day 3 in both ChR2- and ChR2+ rats on the familiar task may be due to the interference of information from the altered task on familiar task performance. Then ChR2- rats' performance improves due to the use of efficient spatial strategies from healthy hippocampal function. However, the adaptation of ChR2+ rats to disrupted hippocampal place cell encoding is to adopt a performance strategy that does not require hippocampal spatial mapping. After day 3, this inefficient procedural strategy produces a behavioral deficit relative to the improving ChR2- controls. We postulate that ChR2+ rats do not return to a hippocampal strategy as there is little motivation to attempt a strategy shift; i.e. despite frequent errors, they consume the same number of rewards. Long term hippocampal impairment is not a factor; once the formerly LC stimulated ChR2+ rats were introduced to another hippocampus-dependent task in a different context (the novel task), they were able to learn the task at similar rates to ChR2- rats. Future work is needed to understand why only 2 days of post-learning abnormal LC activity during sleep caused lasting, but context-specific hippocampal deficits.

We propose that LC silences permit sleep spindle generation by preventing noradrenergic depolarization of thalamocortical circuits as depolarization prevents the calcium spikes necessary for spindle generation [20]. Persistent LC activity, as in our study, would decrease spindle occurrence, thereby reducing spindle-ripple related neural activity. Higher frequencies of LC stimulation during sleep used in another study also suppressed ripple-spindle events [51]. LC silences prior to spindles could be key to ripple-spindle coupling and inter-regional communication during memory consolidation [1,2].

We have shown profound learning and memory reconsolidation behavioral deficits with a mild physiological increase in LC cell activity during the sleep consolidation period. We also show subsequent neural coding instability. Together these results likely explain the animals' inability to use a neural code to solve the spatial memory task. More work is required to study the replay patterns and plasticity effects of inappropriate LC activity during sleep consolidation.

In light of our current data, we conclude that LC silences play an important role in spindle generation and ripple-spindle coupling, as well as in normal NREM delta and REM sleep theta rhythm power—oscillations essential to normal offline processing of memory [11,52,57]. Our research suggests that LC activity, or lack thereof, during sleep may play a role in memory expression and be related to memory issues in conditions of abnormal LC activity during sleep such as post-traumatic stress disorder and Alzheimer's disease [53,54].

Author Contributions
K.S., D.B, K.C performed experiments; K.S, B.G, M.F. analyzed data; K.S., G.P. designed experiments; E.V., G.A-J., Y.L., A.P. constructed and provided vectors; S.S. contributed experimental and data analysis expertise; K.S., G.P. wrote the manuscript.

Declaration of Interests
The authors declare no competing interests.

References

1. Wierzynski, C.M., Lubenov, E. V., Gu, M., and Siapas, A.G. (2009). State-Dependent Spike-Timing Relationships between Hippocampal and Prefrontal Circuits during Sleep. Neuron *61*, 587–596.
2. Siapas, A.G., and Wilson, M.A. (1998). Coordinated Interactions between Hippocampal Ripples and Cortical Spindles during Slow-Wave Sleep. Neuron *21*, 1123–1128.
3. Sirota, A., Csicsvari, J., Buhl, D., and Buzsáki, G. (2003). Communication between neocortex and hippocampus during sleep in rodents. Proc. Natl. Acad. Sci. *100*, 2065–2069.
4. Ji, D., and Wilson, M.A. (2007). Coordinated memory replay in the visual cortex and hippocampus during sleep. Nat. Neurosci. *10*, 100–107.
5. Sara, S.J. (2009). The locus coeruleus and noradrenergic modulation of cognition. Nat. Rev. Neurosci. *10*, 211–223.
6. O'Dell, T.J., Connor, S.A., Guglietta, R., and Nguyen, P. V (2015). β-Adrenergic receptor signaling and modulation of long-term potentiation in the mammalian hippocampus. Learn. Mem. *22*, 461–71.
7. Carter, M.E., Yizhar, O., Chikahisa, S., Nguyen, H., Adamantidis, A., Nishino, S., Deisseroth, K., and Lecea, L. De (2010). Tuning arousal with optogenetic modulation of locus coeruleus neurons. Nat. Neurosci. *13*, 1526–1533.
8. Eschenko, O., and Sara, S.J. (2008). Learning-Dependent, Transient Increase of Activity in Noradrenergic Neurons of Locus Coeruleus during Slow Wave Sleep in the Rat : Brain Stem--Cortex Interplay for Memory Consolidation? *Cerebral Cortex.* (8) 2596-2603.
9. Eschenko, O., Magri, C., Panzeri, S., and Sara, S.J. (2012). Noradrenergic Neurons of the Locus Coeruleus Are Phase Locked to Cortical Up-Down States during Sleep. Cerebral Cortex 2, 42-435.
10. Aston-Jones, G., and Bloom, F.E. (1981). Activity of norepinephrine-containing locus coeruleus neurons in behaving rats anticipates fluctuations in the sleep-waking cycle. J. Neurosci. *1*, 876–86.
11. Boyce, R., Glasgow, S.D., and Williams, S. (2016). Casual evidence for the role of REM sleep theta rhythm in contexual memory consolidaiton. Science *23*, 812–816.
12. Nishida, M., and Walker, M.P. (2007). Daytime naps, motor memory consolidation and regionally specific sleep spindles. PLoS One *2*, e341.
13. Mednick, S.C., Mcdevitt, E.A., Walsh, J.K., Wamsley, E., Paulus, M., Kanady, J.C., and Drummond, S.P.A. (2013). The Critical Role of Sleep Spindles in Hippocampal-Dependent Memory : A Pharmacology Study. J. Neurosci. *13*, 4494–4504.
14. Sara, S.J. (2017). Sleep to remember. J. Neurosci. *37*, 457–463.
15. Braunewell, K.H., and Manahan-Vaughan, D. (2001). Long-term depression: a cellular basis for learning? Rev. Neurosci. *12*, 121–40.
16. Manahan-Vaughan, D., and Braunewell, K.-H. (1999). Novelty acquisition is associated with induction of hippocampal long-term depression. Proc. Natl. Acad. Sci. *96*, 8739–8744.
17. Watts, A., Gritton, H.J., Sweigart, J., and Poe, G.R. (2012). Antidepressant Suppression of Non-REM Sleep Spindles and REM Sleep Impairs Hippocampus-Dependent Learning While Augmenting Striatum-Dependent Learning. J. Neurosci. *32*, 13411–13420.
18. Gottesmann, C. (1992). Detection of seven sleep-waking stages in the rat. Neurosci. Biobehav. Rev. *16*, 31–38.
19. Steriade, M., McCormick, D., and Sejnowski, T. (1993). Thalamocortical oscillations in the sleeping and aroused brain. Science. *262*, 679–685.
20. Lee, K.H., and McCormick, D.A. (1996). Abolition of Spindle Oscillations by Serotonin and Norepinephrine in the Ferret Lateral Geniculate and Perigeniculate Nuclei In Vitro. Neuron *77*, 335–350.
21. Li, Y., Hickey, L., Perrins, R., Werlen, E., Patel, A.A., Hirschberg, S., Jones, M.W., Salinas, S., Kremer, E.J., and Pickering, A.E. (2016). Retrograde optogenetic characterization of the pontospinal module of the locus coeruleus with a canine adenoviral vector. Brain Res. *1641*, 274–290..
22. Tamminen, J., Payne, J.D., Stickgold, R., Wamsley, E.J., and Gaskell, M.G. (2010). Sleep spindle activity is associated with the integration of new memories and existing knowledge. J. Neurosci. *30*, 14356–60.
23. Poe, G.R., Thompson, C.M., Riley, B.T., Tysor, M.K., Bjorness, T.E., Steinhoff, B.P., and Ferluga, E.D. (2002). A spatial memory task appropriate for electrophysiological recordings. J. Neurosci. Methods *121*, 65–74.
24. Abel, T., Havekes, R., Saletin, J.M., and Walker, M.P. (2013). Sleep, plasticity and memory from molecules to whole-brain networks. Curr. Biol. *23*, R774–R788.
25. Poe, G.R., Nitz, D.A., Mcnaughton, B.L., and Barnes, C.A. (2000). Experience-dependent phase-reversal of hippocampal neuron firing during REM sleep. Brain Res. *855*, 176–180.
26. Booth, V., and Poe, G.R. (2006). Input Source and Strength Influences Overall Firing Phase of Model Hippocampal CA1 Pyramidal Cells During Theta : Relevance to REM Sleep Reactivation and Memory Consolidation. *173*, 161–173.
27. Mehta, M.R., Barnes, C.A., and McNaughton, B.L. (1997). Experience-dependent, asymmetric expansion of hippocampal place fields. Proc. Natl. Acad. Sci. *94*, 8918–8921.
28. Mehta, M.R., Quirk, M.C., and Wilson, M.A. (2000). Experience-Dependent Asymmetric Shape of Hippocampal Receptive Fields. Neuron *25*, 707–715.
29. Ekstrom, A.D., Meltzer, J., McNaughton, B., and Barnes, C. (2001). NMDA Receptor Antagonism Blocks Experience-Dependent Expansion of Hippocampal Place Fields. Neuron *31*, 631–638.
30. Thompson, L.T., and Best, P.J. (1990). Long-term stability of the place-field activity of single units recorded from the dorsal hippocampus of freely behaving rats. Brain Res. *509*, 299–308.
31. Bjorness, T.E., Riley, B.T., Tysor, M.K., and Poe, G.R. (2005). REM restriction persistently alters strategy used to solve a spatial task. Learn. Mem. *12*, 352–359.
32. Aston-Jones, G., Segal, M., and Bloom, F. (1980). Brain aminergic axons exhibit marked variablility in conduction velocity. Brain Res. *195*, 215–222.
33. Aston-Jones, G., Foote, S.L., and Segal, M. (1985). Impulse conduction properties of noradrenergic locus coerlueus axons pojecting to monkey cerebrocortex. Neuroscience *15*, 765–777.
34. Eschenko, O., Molle, M., Born, J., and Sara, S.J. (2006). Elevated Sleep Spindle Density after Learning or after Retrieval in Rats. J. Neurosci. *26*, 12914–12920.
35. Tamminen, J., Payne, J.D., Stickgold, R., Wamsley, E.J., and Gareth, M. (2011). Sleep spindle activity is associated with the integration of new memories into

existing knowledge. J. Neurosci. *30*, 14356–14360.

36. Kaestner, E., Wixted, J., and Mednick, S. (2013). Pharmacologically increasing sleep spindles enhances recognition for negative and high arousal memories. J. Cogn. Neurosci. *26*, 194–198.

37. Poe, G.R. (2017). Sleep Is for Forgetting. J. Neurosci. *37*, 464–473.

38. Li, W., Ma, L., Yang, G., and Gan, W. (2017). REM sleep selectively prunes and maintains new synapses in development and learning. Nat Neuro. *20*, 427-437.

39. Katsuki, H., Izumi, Y., and Zorumski, C.F. (1997). Noradrenergic regulation of synaptic plasticity in the hippocampal CA1 region. Neurophysiol *77*, 3013–20.

40. Diering, G.H., Nirujogi, R.S., Roth, R.H., Worley, P.F., Pandey, A., and Huganir, R.L. (2017). Homer1z drives homeostatic scaling-down of excitatory synapses during sleep. Science. *515*, 511–515.

41. Stickgold,R., Whidbee, D., Schirmer, B., Patel, V., and Hobson, J.A. (2000). Visual discrimination task improvement: a multi-step process occurring during sleep. J. Cogn. Neurosci. *12*, 246-254.

42. Cahill, L., Prins, B., Weber, M., and McGaugh, J.L. (1994). Beta-adrenergic activation and memory for emotional events. Nature *371*, 702–704.

43. Molle, M., Marshall, L., Gais, S., and Born, J. (2004). Learning increases human electroencephalographic coherence during subsequent slow sleep oscillations. Proc. Natl. Acad. Sci. *101*, 13963–13968.

44. Gazarini, L., Stern, C.A.J., Carobrez, A.P., and Bertoglio, L.J. (2013). Enhanced noradrenergic activity potentiates fear memory consolidation and reconsolidation by differentially recruiting α1- and β-adrenergic receptors. Learn. Mem. *20*, 210–9.

45. Marshall, L., Helgadóttir, H., Mölle, M., and Born, J. (2006). Boosting slow oscillations during sleep potentiates memory. Nature *444*, 610–613.

46. Roozendaal, B., Nguyen, B.T., Power, A.E., and McGaugh, J.L. (1999). Basolateral amygdala noradrenergic influence enables enhancement of memory consolidation induced by hippocampal glucocorticoid receptor activation. Proc. Natl. Acad. Sci. *96*, 11642–7.

47. Fattinger, S., Beukelaar, T.T. De, Ruddy, K.L., Volk, C., Heyse, N.C., Herbst, J.A., Hahnloser, R.H.R., Wenderoth, N., and Huber, R. (2017). Deep sleep maintains learning efficiency of the human brain. Nat. Commun. *8*, 1–13.

48. Przybyslawski, J., Roullet, P., and Sara, S.J. (1999). Attenuation of emotional and nonemotional memories after their reactivation: Role of beta adrenergic receptors. J. Neurosci. *19*, 6623–6628.

49. Kempadoo, K.A., Mosharov, E. V, Choi, S.J., Sulzer, D., and Kandel, E.R. (2016). Dopamine release from the locus coeruleus to the dorsal hippocampus promotes spatial learning and memory. Proc. Natl. Acad. Sci. *113*, 201616515.

50. Wagatsuma, A., Okuyama, T., Sun, C., Smith, L.M., Abe, K., and Tonegawa, S. (2017). Locus coeruleus input to hippocampal CA3 drives single-trial learning of a novel context. Proc. Natl. Acad. Sci.

51. Novitskaya, Y., Sara, S.J., Logothetis, N.K., and Eschenko, O. (2016). Ripple-triggered stimulation of the locus coeruleus during post-learning sleep disrupts ripple/spindle coupling and impairs memory consolidation. Learn. Mem. *23*, 238–248.

52. Maingret, N., Girardeau, G., Todorova, R., Goutierre, M., and Zugaro, M. (2016). Hippocampo-cortical coupling mediates memory consolidation during sleep. Nat. Neurosci. *19*, 959.

53. Berridge, C.W., and Waterhouse, B.D. (2003). T he locus coeruleus – noradrenergic system : modulation of behavioral state and state-dependent cognitive processes. *42*, 33–84.

54. Mellman, T.A., Kumar, A., Kulick-Bell, R., Kumar, M., and Nolan, B. (1995). Nocturnal/daytime urine noradrenergic measures and sleep in combat-related PTSD. Biol. Psychiatry *38*, 174–179.

55. Ghasemi, A., and Zahediasl, S. (2012). Normality tests for statistical analysis: A guide for non-statisticians. Int. J. Endocrinol. Metab. *10*, 486–489.

56. Girardeau, G., Benchenane, K., Wiener, S.I., Buzsáki, G., and Zugaro, M.B. (2009). Selective suppression of hippocampal ripples impairs spatial memory. Nat. Neurosci. *12*, 1222–1223.

57. Walker, M.P. (2009). The role of slow wave sleep in memory processing. J. Clin. Sleep Med. *5*, S20–S26.

58. William E. Skaggs and Bruce L. McNaughton and Katalin M. Gothard and Etan J. Markus (1993). An Information-Theoretic Approach to Deciphering the Hippocampal Code. Proc. IEEE, 1030-1037.

59. Roux, L., Hu, B., Eichler, R., Stark, E., and Buzsáki, G. (2017). Sharp wave ripples during learning stabilize the hippocampal spatial map. Nat. Neurosci. *20*, 845–853.

60. Fuhs, C., Vanrhoads, S.R., Casale, A.E., Mcnaughton, B., Touretzky, D.S., Fuhs, M.C., Vanrhoads, S.R., Casa, A.E., Mark, C., Vanrhoads, S.R., *et al.* (2005). Influence of path integration versus environment orientation on place cell remapping between visually identical environments. J. Neurophysiol., 2603–2616.

MAIN TEXT FIGURE/TABLE LEGENDS

Figure 1. LC spikes sync to peak spindle power and LC optogenetic stimulation decreases spindle occurrence.
(A) Example of LC timing in relation to spindles. LC activity ceases prior to spindle onset, and during the spindle (in blue), LC activity returns leading to a decrease in spindle power.
(B) Normalized root mean square of spindle power (10-15 Hz) during sleep spindles centered on LC spikes. The blue line represents the effect of LC spikes on spindle power when spikes occur within identified spindles, whereas the dark grey line represents the effect of LC spikes on spindle power outside of identified spindle (n=3 rats). The light grey area represents significant different between the two with significance from $p<0.05$ to $P<0.0001$ from t=-0.67 to t=0.54 seconds; displayed as mean ± sem.
(C) Example heat map displaying rise and fall of spindle power centered on LC spikes occurring within the spindles (n=561 spindles, from three animals).
(D) Two Hz LC stimulation during sleep decreases CA1 spindle occurrence rate in ChR2+ rats, n=4. Paired t-test $p=0.0003$ ***$p<0.0005$. Displayed as mean ± sem.
See also Figures S1 and S2.

Figure 2. LC stimulation during sleep impairs next day place field encoding.
(A) Schematic of recording layout and experimental timeline.
(B) The cumulative probability of the lap to lap place field Pearson correlation on altered task. Fields with high spatial stability have a higher correlation. Day 2 ChR2+ rats show a shift towards more fields having lower correlation values. Kolmogorov-Smirnov Test **$p<0.01$. Subplot bar graph displaying the overall average day 2 field correlation. Mann-Whitney $p=0.003$; ***$p<0.005$.
(C) Representative heat maps of place field spatial encoding with lighter colors displaying where CA1 pyramidal spikes were located along the track (horizontally), and where firing occurred across multiple laps (vertically). Top two represent lower correlation fields from ChR2+ Day 2. Bottom two represent higher correlation fields from ChR2- day 2.
(D) Average place field shift per lap on the altered task on Day 1 and Day 2. As shifts can be in positive or negative direction, the absolute value of the shifts are used to calculate the averages in part B and D. Part A and C: ChR2- Day 1 n=61, ChR2+ Day 1 n=43, ChR2- Day 2 n=45, ChR2+ Day 2 n=31 (outlier removed from Control Day 1 and Control Day 2). Kruskal-Wallis, Dunn post hoc: ChR2+ day 1 vs ChR2+ day 2 $p=0.040$, ChR2- day 2 vs ChR2+ day 2 $p=0.013$; *$p<0.05$.
(E) The average lap to lap place field correlation on familiar task with ChR2 Day 2 rats showing decreased field correlation. Kolmogorov-Smirnov Test **$p<0.01$. Subplot bar graph displaying the overall average day 2 field correlation. Mann-Whitney $p=0.023$; *$p<0.05$.
(F) Representative heat maps of place field spatial encoding on the familiar task. Top two represent lower correlation fields from ChR2 Day 2. Bottom two represent higher correlation fields from Control Day 2.
(G) Average place field shift per lap on the familiar task on Day 1 and Day 2. Part D and G: Control Day 1 n=66, ChR2 Day 1 n=40, Control Day 2 n=37, ChR2 n=32 (one outlier removed from Control Day 2). Kruskal-Wallis, Dunn post hoc: ChR2- day 2 vs ChR2+ day 2 $p=0.046$; *$p<0.05$. Bar graphs displayed as mean ± sem.
See also Figure S3

Figure 3. LC stimulation during sleep impairs learning and memory.
(A) The average errors per lap by day for the ChR2- and the ChR2+ groups on the altered task. Two-way ANOVA, Sidak post hoc (in black): ChR2- vs ChR2+ day 4 $p=0.0012$, day 5 $p=0.0017$. Two-way ANOVA, Tukey post hoc (in yellow): ChR2- day 1 vs day 5 $p=0.002$. **$p<0.005$.
(B) The average errors per lap for ChR2- and stimulated ChR2+ group on the familiar task. Two-way ANOVA, Sidak post hoc (in black): ChR2- vs ChR2+ day 4 $p=0.0032$, day 5 $p=0.0004$. Two-way ANOVA, Tukey post hoc (in blue): ChR2+ day 1 vs day 5 $p<0.0001$.
(C) The average errors per lap for ChR2- and ChR2+ groups on the novel task with both groups meeting criteria of less than one error per lap after three days of maze running. Two-way ANOVA, Tukey post hoc: ChR2- day 8 vs day 10 (in yellow) $p=0.0019$, ChR2+ day 8 vs ChR2+ day 10 (in blue) $p=0.0084$. Five rats for each group for part A and B; three rats for each group in part C. Data displayed as mean ± sem. *$p<0.05$ **$p<0.005$, ***$p<0.0005$, ****$p<0.0001$.

Figure 4. LC stimulation during sleep alters maze solving strategies
(A) Schematic showing difference between procedural errors and map errors. Red dots would be map errors on the familiar task as they are only baited during the altered task, and blue dots represent map errors on the altered task as those boxes are only baited on the familiar task. Purple dots are boxes that are consistent whether baited or non-baited between the familiar and the altered task.
(B) ChR2- group altered task performance broken down by error type. Two-way ANOVA, Sidak post hoc: map vs procedural errors day 1 $p<0.0001$, day 2 $p=0.0012$, day 3 $p=0.0012$, day 4 $p=0.0001$, day 5 $p=0.0009$. *$p<0.005$.
(C) ChR2+ group performance on the altered task broken down by error type. Two-way ANOVA, Sidak post hoc: map vs procedural errors: day 1 $p=0.0016$. *$p<0.005$.
(D) ChR2- group performance on the familiar task broken down by error type. Two-way ANOVA, Sidak post hoc: map vs procedural errors day 3 $p=0.01$, day 4 $p=0.0047$. *$p<0.05$
(E) ChR2+ performance on the familiar task broken down by error type. Five rats in each group for part B-E. Dots and error bars represent day mean± sem.

Figure 5. LC stimulation does not produce changes in sleep architecture but does alter spectral power.
(A) The percent time spent awake and sleeping compared to total time
(B) The percent of total sleep spent in slow wave sleep, in intermediate sleep, and in REM sleep.
(C) The number of transitions from NREM sleep to wake and REM sleep to wake within the first hour of sleep.
(D) Percent change from baseline to Day 1 in CA1 LFP spectral power during waking, slow wave sleep, intermediate sleep, REM sleep. Five control rats, four ChR2 rats for part A-D. Two-way ANOVA, Sidak post hoc. Bars represent mean ± sem.
(E) Percent change in band power from baseline to day 1 sleep. δ 1-4 Hz, θ 5-9 Hz, σ 10-15 Hz, β 16-20 Hz, γ^{slow} 30-50, γ^{fast} 61-100 Hz for all figures. Two-way ANOVA, Sidak post hoc: SWS delta $p=0.0067$; IS delta $p=0.0007$ sigma $p=0.0009$; REM theta $p=0.005$. *$p<0.05$, **$p<0.01$, ***$p<0.005$.

Figure 6. Changes in REM sleep theta power and NREM spindle occurrence from baseline sleep to day 1 sleep with LC stimulation.
(A) The percent change from baseline to day 1 in REM sleep theta power vs day 5 altered task total errors (left) and day 5 familiar task total errors. ChR2+ vs ChR2- change in REM theta (x axis comparison) Mann-Whitney $p=0.0079$. ChR2+ vs ChR2- altered task errors (y axis comparison) Mann-Whitney $p=0.008$. ChR2+ vs ChR2- familiar task errors (y axis comparison) Mann-Whitney $p=0.016$.
(B) The percent change from baseline to day 1 in CA1 spindle occurrence during NREM sleep vs day 5 altered task total errors (left) and day 5 familiar task total errors. ChR2+ vs ChR2- change in spindle rate (x axis comparison) Mann-Whitney $p=0.016$. ChR2+ vs ChR2- altered task errors (y axis comparison) Mann-Whitney $p=0.008$. ChR2+ vs ChR2- familiar task errors (y axis comparison) Mann-Whitney $p=0.016$. Error bars represent the minimum and maximum within a data set; vertical and horizontal lines cross at the mean from each group, marked with symbols for both A and B.
(C) The effect of LC stimulation on CA1 sigma power within spindles. Normalized CA1 sigma power is shown in relation to light stimulation events within spindles (n=700). Events were then shuffled within spindles to preserve spindle specificity for ten shuffled data sets of 700 shuffled events each. A two-way ANOVA, Sidak post hoc was calculated for the real data (n=700 events) vs. each shuffled set individually (n=700 per set), and then against the average of all ten shuffles. The effect of light stimuli was nonrandom (p<0.05 from shuffled) for t= -0.04 to 0.18 for all individual and the combined two-way ANOVAs. Light stimulation significantly reduced sigma RMS; two-way ANOVA, Dunnett post hoc light onset t=0 vs t>0. #p<0.05 at t=0.088 seconds and onward.
(D) The percent change in occurrence of spindles greater or less than 0.6 seconds in length. Two-way ANOVA, Sidak post hoc ChR2- vs ChR2+ $p=0.013$ Data displayed as mean ± sem. *$p<0.05$, **$p<0.01$.
See also Figure S4 and Table S1.

Figure 7. LC stimulation during sleep interferes with ripple-spindle coupling.
(A) Spindle onset probability displayed in respect to ripple onset at t=0 during baseline sleep. Ripple onset timestamps were shuffled within NREM sleep periods with no repeating timestamps within trials, and were shuffled for a total of 15 trials to ensure coupling was non-random. Two-way ANOVA, Sidak post hoc; ChR2+ vs

ChR2+ shuffled p<0.0001; ChR2- vs ChR2- shuffled p<0.0001. There was no difference between the shuffled values for ChR2+ and ChR2- groups (p=0.997), therefore only ChR2+ shuffled values are displayed for visual purposes. Any probability within the gray region represents random for both ChR2+ and ChR2-. As there was no difference between either groups shuffled data in part B as well (p=0.958), within part B the gray region represents both ChR2+ and ChR2- shuffled data.

(B) Spindle onset probability displayed in respect to ripple onset at t=0 during Day 1 sleep with 2 Hz LC stimulation. Two-way ANOVA, Sidak post hoc; ChR2+ vs ChR2+ shuffled p<0.0001; ChR2- vs ChR2- shuffled p<0.0001. ChR2- vs ChR2+ from t=-50 to -250 msec p<0.0001. ChR2-=4, ChR2+=5 ***p<0.0001. Displayed as mean (line) ± sem (shaded region).

See also Figure S5.

STAR METHODS

CONTACT FOR REAGENT AND RESOURCE SHARING

Further information and request for resources may be directed to the Lead Contact and corresponding author, Gina Poe (ginapoe@ucla.edu).

EXPERIMENTAL MODELS AND SUBJECT DETAILS

A total of twenty-six male Long-Evans rats (Charles River), age 4-5 months and weighing approximately 350-400g were individually housed in cages (45.7 x 24.1 x 20.3 cm) with shaved cellulose bedding, climate controlled (23 ± 3°C and 40 ± 10% humidity) and with 12:12 hour light/dark cycle. Food and water were available *ad libitum* prior to food restriction during behavioral training. All animal procedures were carried out in accordance with the National Institutes of Health Guide for the Care and Use of Laboratory Animals and in accordance with the University of Michigan Committee on the Use and Care of Laboratory Animals.

METHOD DETAILS

Viral Injection
Animals were orally administered (20 mg/kg) ciprofloxacin and liquid acetaminophen (orally 30ml/150 ml water) 24 hours prior to surgery. Rats were anesthetized with isoflurane vapor (4% induction, 1-2% maintenance) and placed in a stereotaxic frame. All stereotaxic measurements were from bregma. A vector expressing a light sensitive channelrhodopsin-2 (ChR2) under the control of PRSx8 (synthetic dopamine beta hydroxylase promoter), lenti-PRSx8-ChR2-mCherry or CAV2-PRSx8-ChR2-mCherry (Li et al., 2016), or a control vector, AAV-PRSx8-mCherry, was bilaterally injected (1.2 µl) into the locus coeruleus (AP -12.1 mm; ML ±1.3mm; DV 6.1 mm at 20°) through 30-gauge injection cannula at a rate of 0.2 ml min^{-1} for 6 minutes. Post-injection, needles were left in tissue for 10 minutes prior to removal.

Electrode Implantation
LC and CA1 single cell recordings were collected with dual eight independently movable tetrodes (groups of four twisted microwires) microdrives. The anterior microdrive contained two bilateral cannula containing four tetrodes each targeting the hippocampus (from bregma: -4.0 mm AP; ± 2.5 mm ML; - 2.0–2.5 mm DV). The posterior microdrive contained two bilateral cannula containing four tetrodes each targeting the LC (from bregma: AP -12.1 mm; mediolateral ML ±1.2mm; DV -6.1 mm at 20° to avoid the transverse sinus). A screw electrode (Plastics One) was implanted over the prefrontal cortex (from bregma: +2.0 mm AP; ± 2.0 mm ML) to be used as a ground. Two nuchal electromyographic (EMG) electrodes were implanted into the dorsal neck muscles. All implanted tetrodes were used to measure local field potential (LFP) and detect single unit activity. Anchor screws and dental cement were used to adhere implants to the skull.

Behavioral Training and Motivation
Rats were trained on an octagonal version of an eight-box spatial learning task originally developed in our lab (Poe et al., 2002). Eight boxes were positioned with one at each corner of an elevated octagonal track. Each box consisted of a reward reservoir that is hidden behind a hinged door that must be opened to reach the food reward (Ensure® Abbott Labs, Columbus, OH). Each reservoir was fed by a plastic tube coupled to a syringe allowing the observer to fill reservoirs without interacting with the maze. Below each box, an inaccessible compartment was baited with Ensure so that all boxes smelled as though they contain a reward to prevent use of olfaction to locate the reward.

Rats were food restricted to >85% of their free feeding weight and trained daily at ZT 0.5 (30 minutes into the light phase) in 30 minute sessions. Rats were trained to run clockwise on the track and locate the three of eight boxes that contained a food reward (0.5 mL Ensure) using static visual cues in the room. A training session consisted of three 5-lap trials (totaling 15 laps). Following a trial of five complete laps, the animal was removed from the maze and placed in a towel lined box for two minutes to encourage animals to use hippocampal-dependent learning and not working memory. During these two minutes, reservoirs were cleaned of food residue, and the maze was rotated

(minimum 45 degrees, max 180 degrees). In all trials, reward boxes were located at the same allocentric locations with respect to visual cues of the room. At the beginning of each trial, rats were reintroduced to the maze at different locations to prevent learning reward location relative to initial placement on the maze.

Rats were trained on this familiar layout until they reached the defined performance threshold criterion of averaging less than one error per lap (16.1 ± 1.2 days). Errors consisted of skipping a reward box and checking a non-reward box. Animals were then implanted as described above in *Electrode Implantation,* above. Following 10 days of surgical recovery in their home cages, animals were reintroduced to the maze with the familiar layout, now tethered for electrophysiological recording, and retrained until they met the performance criterion threshold again.

Behavioral Protocol and Rectangular Maze
The experimental protocol consisted of rats running 15 laps on the familiar layout, followed by a 20-minute break from the maze in a towel lined box. Light intensity in the room was kept low during running to minimize animal anxiety and optimize video tracking of the animal through headstage-mounted LEDs. Light was increased during the break between mazes as a cue for maze change. After the break, the lights were returned to low intensity and rats were run 15 laps in three trials on the reversal maze where two of the three previous locations of the food were changed. In addition to counting total errors per lap, error type was also characterized. As two box positions changed between familiar and reversal mazes, there are four potential errors that could be made at those four boxes and they were termed "maze choice" errors. Four potential "static errors" could be made at the four box positions that were never changed between mazes. Thus the probability of either error type being made at random on either the familiar or reversal mazes is 0.5. Errors occurring at positions that remained static between mazes indicate an impaired hippocampal-dependent memory or perhaps abandonment of the hippocampal spatial strategy, whereas errors at baited positions that alternated between familiar and reversal mazes indicate confusion between familiar and reversal maze maps. This 15-lap familiar, 20-minute break, 15-lap reversal was run days 1-5.

Rats were given a break from running on days 6 and 7 and fed their normal restrictive diet. day 8-10, animals were run on a rectangular maze with eight boxes (Poe et al., 2002), three of which contained food, similar to the days 1-5 exercise, only in a different room with different visual cues. Animals were run for three days to determine their ability to learn a new maze to the same criterion of less than one error per lap.

Electrophysiological Recording
Electrode data were recorded at a sampling rate of 32 kHz using Neuralynx Digital Lynx system (Neuralynx, Bozeman, MT). Hippocampal CA1 spikes were detected in real-time from 600 Hz to 6 kHz filtered continuously sampled tetrode data using amplitude threshold crossing. LC spikes were detected in the same manner, but with a 300 Hz to 6 kHz filter.

Tetrode placement in CA1 of the hippocampus was confirmed by moveable tetrode depth, as well as by waveform shape, frequency and audio-converted sound of pyramidal neural spikes. Tetrode placement in the LC was confirmed using calculated moveable tetrode depth, LC firing frequency i.e. relatively low firing during waking and silent during REM sleep quiescence (Aston-Jones and Bloom, 1981), responsiveness to acoustic stimuli (Sara and Segal, 1991), and broad action potential waveform shape.

LC Optical Stimulation
All photostimulation experiments were conducted bilaterally. Two high powered blue LEDs (470 nm Luxeon) were coupled to optical fibers (200 mm core diameter, ThorLabs) using clear optical-grade epoxy (EPOTECH spectral transparency >99% 380-980nm) and implanted targeting the LC (same coordinates as tetrodes). Light pulses from LEDs were generated using a waveform generator (Agilent 3320A arbitrary waveform generator). Generated light pulses were 15 msec in duration and had a consistent 5-10 mW intensity at the fiber tip prior to implantation. *In vivo* confirmation of light evoked potentials from ChR2 expressing LC cells was confirmed with LC tetrode recordings (Figure S2B).

LC stimulation and Arousal Experiments
Frequencies 4 Hz and above of LC optogenetic stimulation during NREM sleep decreased the animal's latency to arousal. SI Appendix Figure S2C shows example LFP spectral heatmaps and EMG traces in response to light

stimulation during NREM sleep in ChR2- and a ChR2+ rats. Only ChR2+ rats arose from NREM sleep, and the effect only occurred in response to light stimulation at 4 Hz frequencies or greater, which was confirmed by increased EMG activity and a power spectral density shift from slow wave delta power (0.4-4 Hz) to waking theta power (5-9 Hz) in the hippocampal CA1 LFP (Figure S2C middle). Light pulses at any frequency were insufficient to produced arousal in ChR2- rats. 1-3 Hz LC stimulation was incapable of awakening the ChR2+ rats from NREM sleep (Figure S2D). We therefore chose a 2 Hz LC stimulation frequency in order to maintain sleep continuity and avoid inducing arousals in ChR2 rats, a sub-arousal threshold frequency that we used in all subsequent experiments. As spontaneous LC firing rates vary from 0-20 Hz, our evoked <2 Hz activity rate was well within physiological parameters and similar to previous work [7].

Histology
Rats were anesthetized with 1.0 mL sodium pentobarbital (intraperitoneal injection), then transcardially perfused through the left ventricle with 150 mL phosphate buffered saline (1X PBS) followed by 150 mL 10%formalin. The brain was removed and placed in 10% formalin for 24 hours, and then in 1x PBS solution containing 30% sucrose for 48-72 hours. Brains were sectioned into 50 μm coronal sections on a cryostat and then washed for 10 min in 1x PBS three times. The sections were blocked for 30 min in a solution containing 0.5% Triton, followed by 30 min in 5% normal goat serum. Primary antibodies for tyrosine hydroxylase (TH), 1:500 mouse-anti-TH (Immunostar), and mCherry (1:500, rabbit anti-mCherry; Biovision) were applied for 24 hours at 4 °C, followed by 1 hour at room temperature (~23 °C). After three 10-min washes with 1X PBS, secondary antibodies (1:1000, Goat anti-Rabbit AlexaFluor-594 and 1:1000, Goat anti-Mouse AlexaFluor-488, Fisher) for were applied for 24 hours at 4 °C. After three 10-min washes with 1X PBS, sections were mounted to slides (Fisher Superfrost Plus) with the ProLong Gold Antifade mounting medium (Invitrogen). Images of antibody stained sections were acquired with an Olympus BX-51 fluorescence microscope using wide-field mode.

QUANTIFICATION AND STATISTICAL ANALYSIS

All statistical tests were conducted in Prism 7 analytical software (GraphPad). All data sets were first tested for normality using Shapiro-Wilk normality test as recommended [55]. Data set normality was calculated without performing any transform (e.g. log10, or z-score) on the data set. Outliers were removed using ROUTs outlier test in Prism 7 with Q=1%. Statistical tests including ANOVA, Pearson correlations, t-tests, and their non-parametric equivalents were performed in a similar matter to previous research. Post-hoc analysis to adjust for multiple comparisons was used in accordance with Prism 7 statistical guide. Alpha was set to 0.05 for all analyses and was always calculated in a two-tail manner. Graphical representations of data were created using Graphpad Prism 7 and MATLAB.

Behavioral Task Performance
Animals' total errors on the familiar and altered task divided by 15 laps to show the average number of errors per lap and analyzed using repeated measures two-way ANOVA (Sidak post-hoc) for performance within a group across days and two-way ANOVA (Tukey post-hoc) for comparing between groups. For the difference between map errors and procedural errors the total number of each type of error was analyzed rather than error per lap. A repeated measures two-way ANOVA (Tukey post-hoc) was used to analyze within each error type and a two-way ANOVA (Sidak post-hoc) was used to compare both types of errors.

Sleep State Analysis
Sleep/waking states were scored manually using CA1 LFP and EMG recordings in the same manner as Emrick et al., 2016. As the present study focuses on hippocampal learning and sleep, and previous work from our lab showed that the cortex and the hippocampus can be in two different sleep states simultaneously (Emrick et al., 2016), CA1 LFP recordings were used instead of cortical EEG for sleep scoring and spindle identification. LFP and EMG recordings were down-sampled to 1000 Hz Epochs (10 s) were assigned a state of active waking, slow-wave sleep (SWS), Intermediate Sleep (which is a non-REM sleep state with high spindle power and occurrence equivalent to Stage 2 non-REM sleep in humans), or REM sleep using a sleep scoring program developed in our lab (Gross et al., 2009). The percentage of time spent in sleep across days within each group and between groups was analyzed using a two-way ANOVA (Sidak post-hoc).

Power Spectral Band Analysis

Down-sampled raw LFP from intervals of each scored state were entered into Neuroexplorer 5 software (Nex Technologies, Madison, AL). LFP data underwent a Fast-Fourier transform (FFT) using a window with a Hann taper. Change from baseline was identified using raw spectral power normalized to baseline across bands and expressed as a percent change from baseline by: ((day 1 – Baseline/Baseline) * 100%). The percent change from baseline to day 1 sleep in the full power spectra and the specific bands was analyzed using a two-way ANOVA (Sidak post hoc). The percent change from baseline to day 1 in REM sleep theta power was analyzed further in figure 6 was analyzed via Mann-Whitney test.

Sleep Spindle and Ripple Identification

Sleep spindles were identified automatically from the entire sleep record. Automatic spindle identification was performed according to Eschenko et al 2006 [34]. Briefly, the sigma frequency (10-15 Hz) was filtered in the CA1 LFP data down-sampled to 200 Hz, taking the root-means-square (RMS) over a 100 msec window, then smoothing it with a moving average. Spindles were counted from periods at least 0.3 s in length where the RMS exceeded three times the standard deviation of the RMS mean of all NREM sleep intervals. Reduction in NREM sleep spindle occurrence from baseline to 2 Hz stimulation was analyzed via paired t-test in Figure 1. The percent change in spindle occurrence between baseline and day 1 was analyzed via Mann Whitney Test in Figure 6.

Ripples were automatically identified similar to the methodology described in Girardeau et al 2009 [56] using a custom script written in MATLAB. Using the RMS of the 100-200 Hz bandpass filtered LFP, ripples were identified when the RMS crossed an upper threshold of five times the standard deviation of the average RMS for NREM and IS sleep. Ripple edges were detected when the RMS fell below a second threshold of two times the RMS standard deviation. Ripples were considered only in segments corresponding to NREM sleep states. Ripple occurrence and ripple length between groups and days was analyzed with a two-way ANOVA (Sidak post hoc) whereas percent change in ripple length and occurrence from baseline was analyzed via Mann Whitney Test.

Ripple-Spindle Coupling

Spindles and ripples were automatically identified (see previous section). Using custom MATLAB scripts, peri-event time histograms (PETHs) were generated using the start time of ripples as the event, and the start time of the spindles as the as the corresponding response. A range of 2500 msec prior to and following ripple onset was used, and bins were 50 msec in width. The number of spindle start times per bin was then divided by the total number of events (ripple start times) to convert to normalized probability. To test that this ripple-spindle coupling was non-random, shuffled ripple start time data (n=15 per animal per day) was generated using a Monte Carlo method similar to Siapas 1998 [2] (we note this is a method of shuffle can be liberal). Shuffling was performed only during periods of NREM sleep to prevent an artificial reduction in the shuffled correlations. Spindle probability between ChR2- and ChR2+ rats, as well as either group vs shuffled data was analyzed using via two-way ANOVA (Sidak post hoc).

Single Unit Isolation

Spike data were sorted into individual neurons using Offline Sorter x64 V3 (Plexon). For each tetrode recording of spikes, the data was manually sorted into single units using spike features of each of the four channels of the tetrode (e.g. principle component analysis or peak amplitude of each channel). LC call and CA1 pyramidal cell firing rate by state was analyzed using a repeated measures two-way ANOVA with Sidak post hoc.

Place Cell Identification and Analysis

Following unit isolation, CA1 units were first separated into pyramidal cells and fast spiking interneurons based upon firing rate while the animal was running on the maze, as well as by spike width (pyramidal cells having a wider spike than fast-spiking interneurons). Interneuron data was then discarded from future analysis. Position tracking data from the rats running on the octagonal tract was separated into laps for the familiar and altered task. The track was then broken into 3 cm bins and linearized. Pyramidal cell spiking data was then used to generate raw rate maps and occupancy maps. Periods of less than 5 cm/s velocity were removed. Information content was calculated as in Skaggs et al. 1993 [58]. Cells with less than an information content of 0.15 were removed similar to Fuhs et al [60] and all cells that were not active a minimum of five laps on a maze were also discarded. A Gaussian smoothing filter (SD=4) was then applied to the firing rate data. Cells were determined to be place cells if their smoothed firing rate crossed threshold (1 Hz) for 3 or more consecutive 3 cm bins, in addition to meeting the above criteria. Place cell stability or lap to lap correlation (r), was computed per cell via a bin-by-bin Pearson's correlation
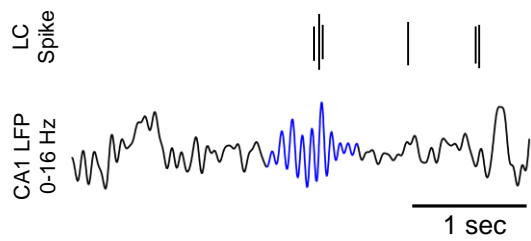
between firing rate maps for all laps that the cell was active similar to [59]. Place cell average lap to lap correlation cumulative probability was analyzed using K-S test, and average day 2 place field lap to lap correlation were analyzed via Mann-Whitney test. Place field absolute shift and size were analyzed using a Kruskal Wallis (Dunn post hoc) and place field center of mass shift from original position was analyzed using a two-way ANOVA (Dunnett post hoc).
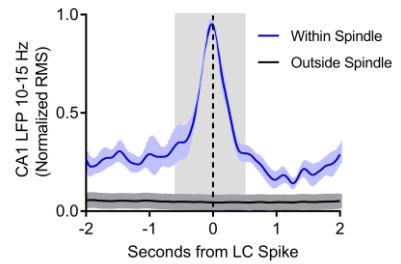
KEY RESOURCES TABLE

REAGENT or RESOURCE	SOURCE	IDENTIFIER
Antibodies		
Mouse monoclonal anti-Tyrosine Hydroxylase	Immunostar	Cat#: 22941
Rabbit polyclonal anti-mCherry	Biovision	Cat#: 5993
Goat AlexaFluor488 anti-mouse	Fisher	RRID: AB_2633275
Goat AlexaFluor594 anti-rabbit	Fisher	RRID: AB_2534095
Bacterial and Virus Strains		
CAV2-PRS-ChR2-mCherry	Montipellier Vector Core	N/A
Lenti-PRS-ChR2-mCherry	This paper	N/A
Chemicals, Peptides, and Recombinant Proteins		
Isoflurane	Zoetis	N/A
10% Formalin	VWR	N/A
Prolong Gold Antifade Agent	Invitrogen/Fisher	Cat#: P36930
Experimental Models: Organisms/Strains		
Long-Evans Male Rats	Charles-River	Strain Code:006
Software and Algorithms		
Matlab v 2017a	Mathworks	RRID:SCR_001622
Offline Sorter 3D v 3.3.2	Plexon	RRID:SCR_000012
NeuroExplorer 5	Neuroexplorer	RRID:SCR_001818
Prism 7	Graphpad	RRID:SCR_002798
Other		
Stereotaxic Apparatus	World Precision Instruments	N/A
Tetrode Wire	Sandvik	Cat#: PX000029
Stainless steel EMG wire	Cooner Wire	Cat#: AS636
Ground Screws	Invivo1	Cat#: E363/20/SPC
Digital Lynx	Neuralynx	DigitalLynx 4SX Upgrade
Cryostat	Leica	CM 1950
Fluorescent Microscope/Camera	Olympus	BX-51

Figure

A

LC
Spike

CA1 LFP
0-16 Hz

1 sec

B

CA1 LFP 10-15 Hz
(Normalized RMS)

Within Spindle
Outside Spindle

Seconds from LC Spike

C

Frequency (Hz)

Power/Frequency

Time from LC Spike (sec)

D

NREM Sleep

Spindles/Sec

***

Baseline
Sleep

Sleep+
2 Hz

Figure

Figure

A Altered Task

Errors/Lap

ChR2−
ChR2+

** **

**

Day

B Familiar Task

Errors/Lap

ChR2−
ChR2+

****

** ***

Base 1 2 3 4 5
Day

C Novel Task

Errors/Lap

ChR2−
ChR2+

*

**

8 9 10
Day
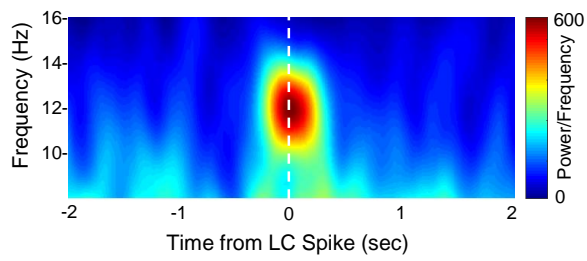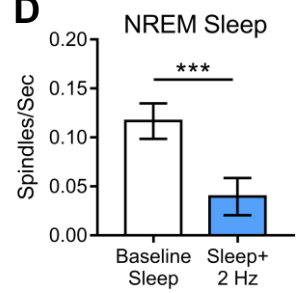
Figure

Figure

Figure

A

Theta vs Altered Task Errors

Theta vs Familiar Task Errors

B

Spindles vs Altered Task Errors

Spindles vs Familiar Task Errors

C

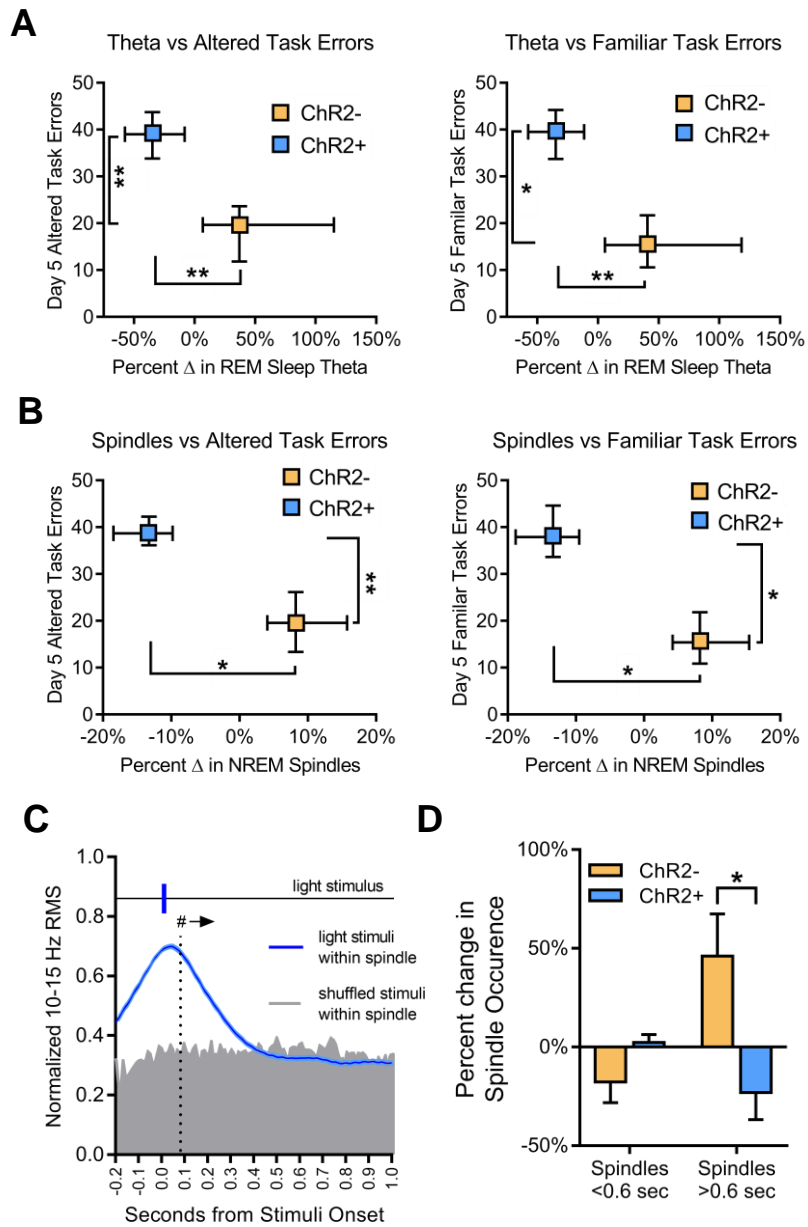**D**

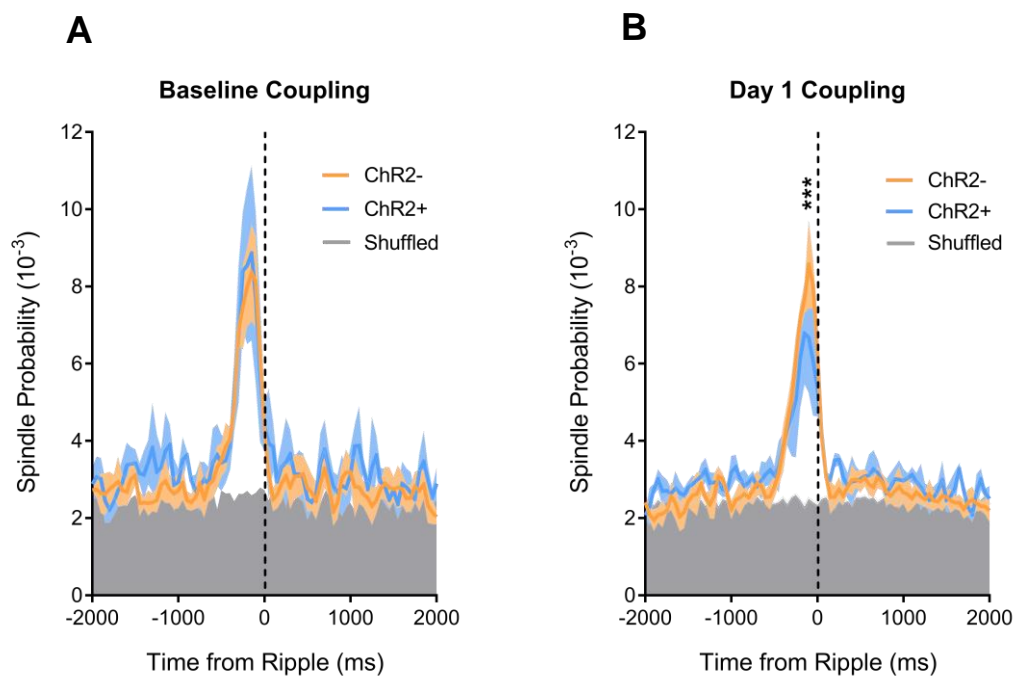Figure

A

Baseline Coupling
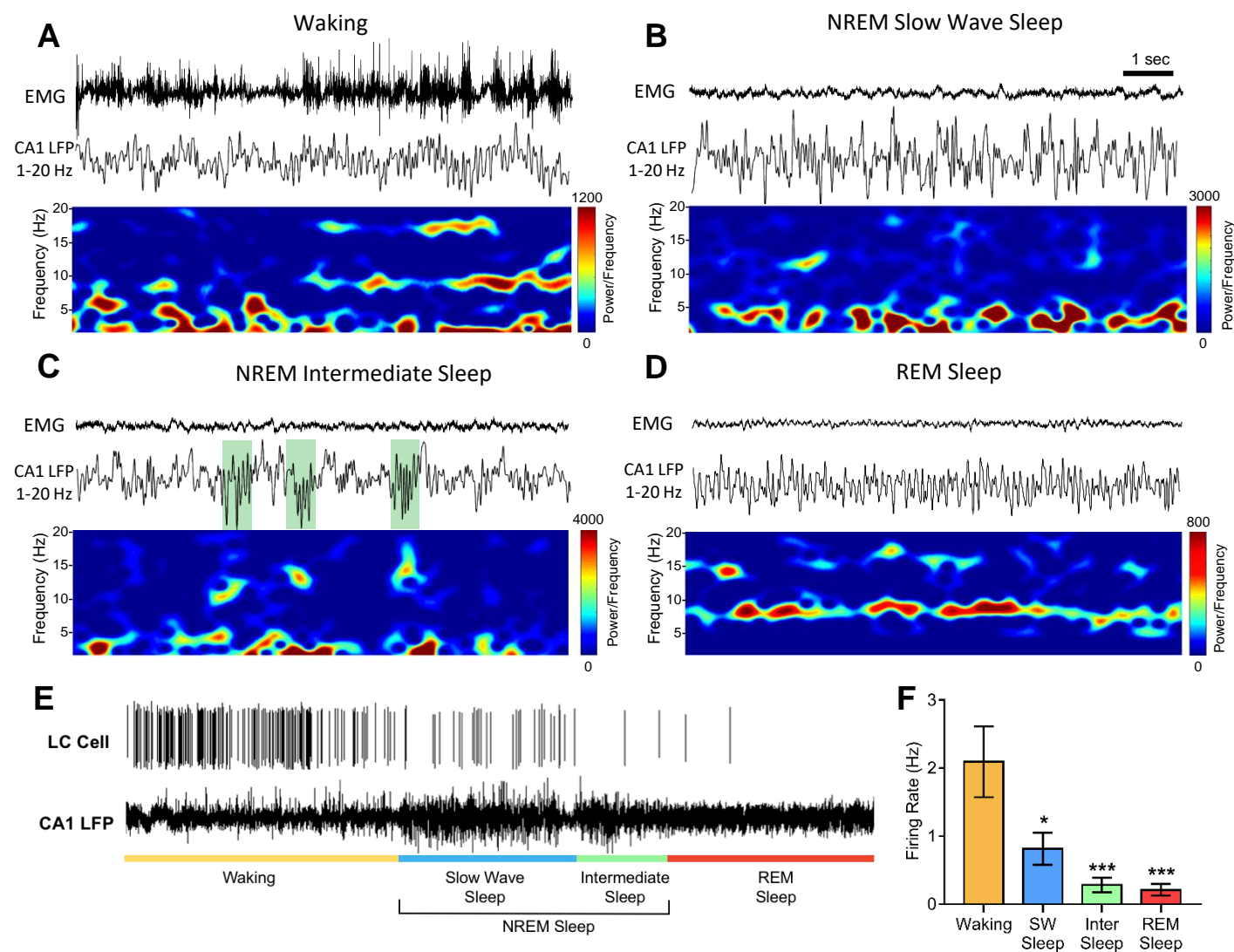

B

Day 1 Coupling

Figure S1. Example 10 second epochs of each scored state of sleep with neck EMG and CA1 LFP (0-20 Hz) and LC spiking activity. Related to Figure 1

(A) Waking with high EMG activity and CA1 theta (5-9 Hz) activity.

(B) NREM slow wave sleep with low EMG activity and characteristic slow waves (0.4-4 Hz).

(C) NREM intermediate sleep that also has low EMG activity, and slow waves but also contains a high occurrence of sleep spindles highlighted in green (spindles can also occur in SWS).

(D) REM sleep with the lowest EMG activity and characteristic high power theta activity and the absence of slower frequency activity that pervades NREM sleep.

(E) Representative example of LC cell spiking activity across different states of waking and sleep as identified by CA1 LFP.

(F) Quantified LC firing rate across different states of sleep compared to waking (in wild type rats). Bar colors match designated state colors in part A. n=12 cells from five rats; comparison of each state vs waking. One-way ANOVA, Tukey post hoc: waking vs SWS p=0.019; waking vs. inter sleep p=0.0004; waking vs. rem sleep p=0.0003. *p<0.05, ***p<0.0005.
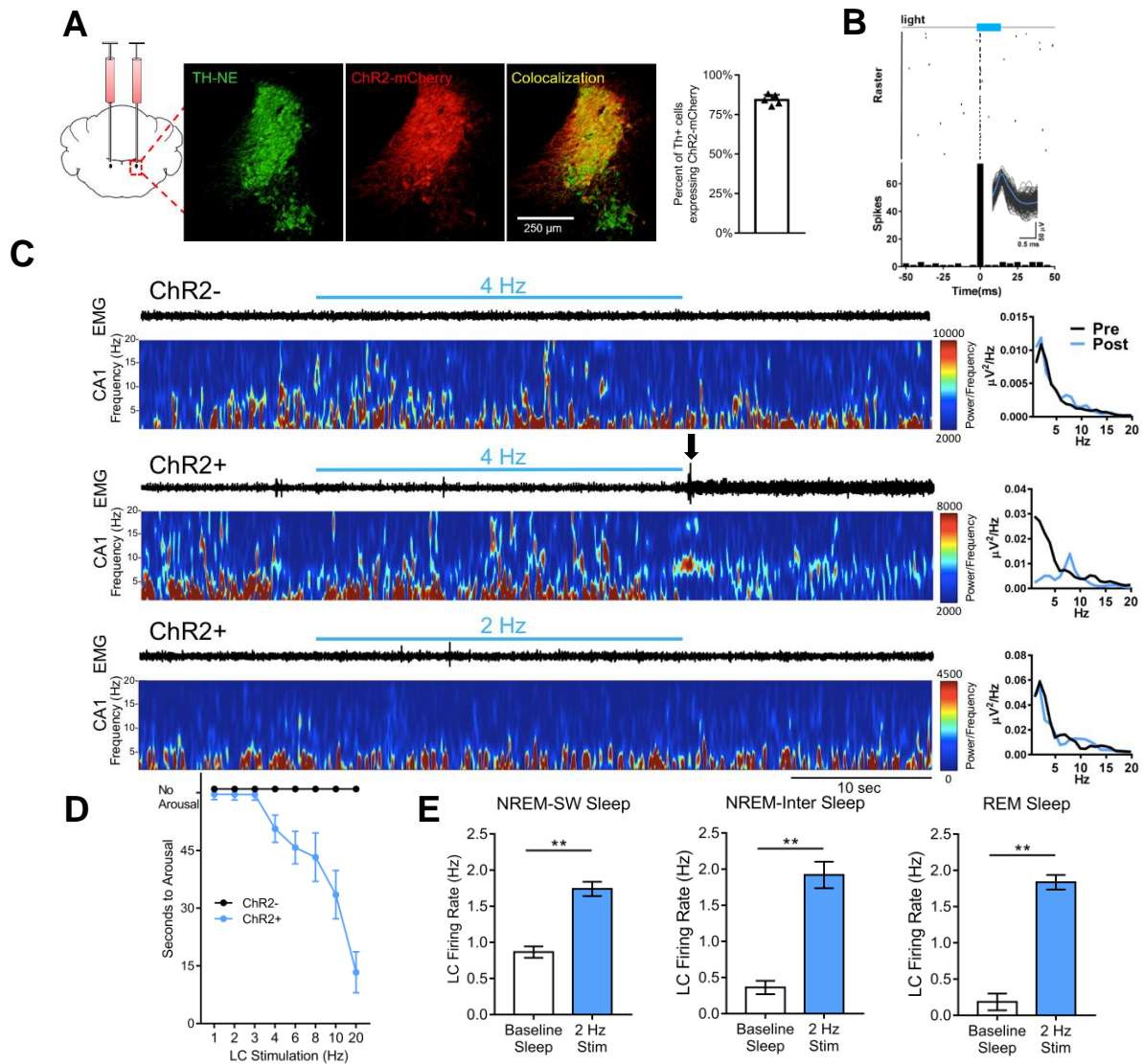
Figure S2. LC stimulation at low frequencies does not generate arousals. Related to Figure 1

(A) Immunostaining of TH-expressing LC cells (green), cells expressing ChR2-mCherry (red), and colocalization of TH and mCherry expressing cells (yellow). Quantification of ChR2-mCherry expression in Th+ cells (n=5 rats).

(B) Perievent raster and spike histogram of LC cells firing in response to 470 nm light stimulation during NREM sleep (75 trials). Subplot of LC spontaneous non-evoked LC waveforms overlaid in grey and the mean of light-evoked LC waveforms shown in in blue.

(C) LFP and EMG traces showing LC optogenetic stimulation effects. The blue bar represents light stimulation with the frequency labeled above. The entire trace length is one minute in length. Top left: 4 Hz stimulation in a control rat showing no arousal. Middle left: 4 Hz stimulation in a ChR2 rat, black arrow shows point of arousal from NREM sleep. Bottom left: 2 Hz stimulation in a ChR2 rat, showing no arousal. The LFP spectral power from the 10 sec pre- and 10 sec post-stimulation are shown to the right of each trace. Arousal following LC stimulation shows clear shift from delta to theta band.

(D) Increasing frequencies of LC stimulation decreases latency to arousal from NREM sleep in ChR2+ rats; ChR2- n=5, ChR2+ n=8.

(E) The change in LC firing rate between baseline and 2 Hz optogenetic stimulation across slow wave sleep, intermediate sleep, REM sleep. Baseline sleep n=5; 2 Hz stim n=8. SWS baseline vs 2 Hz Mann-Whitney p=0.0016; intermediate sleep baseline vs. 2 Hz Mann-Whitney p=0.0016; REM sleep baseline vs. 2 Hz Mann-Whitney p=0.0016. **p<0.005; bars represent mean ± sem.
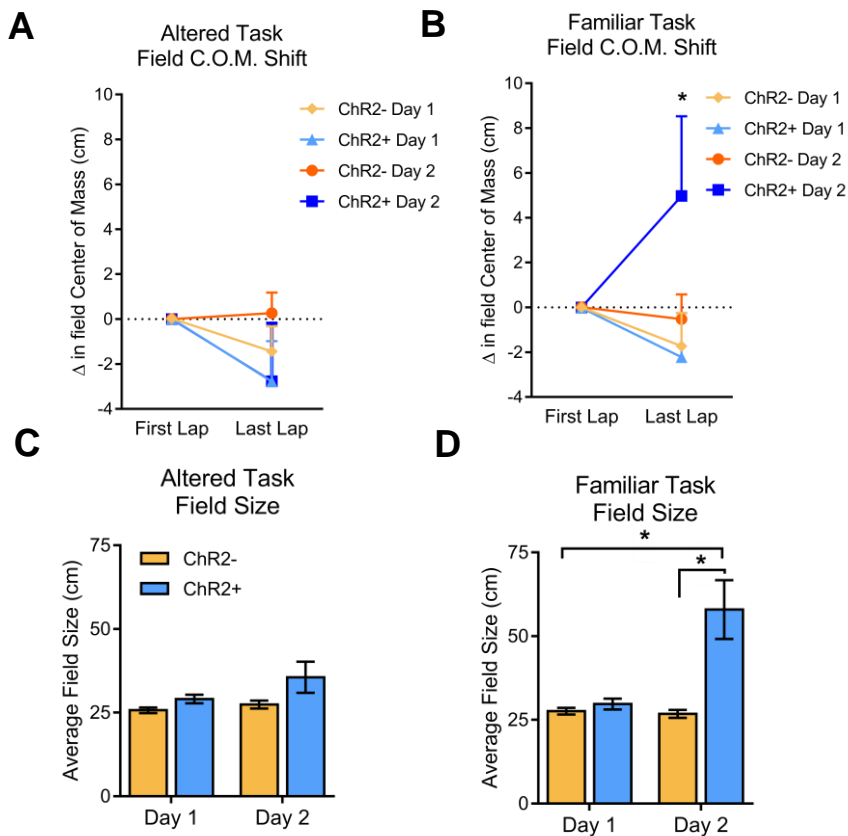
Figure S3. LC stimulation during sleep leads to abnormal place field expansion on the familiar task during next day task performance. Related to Figure 2

(A) Place field center of mass shift from the original position on the first lap to the last lap of the altered task. Both groups expand backwards as previously shown on day 1 and there was no difference between groups on day 2.

(B) Place field center of mass shift from original position on the first lap to the last lap of the familiar task. Both groups expand backwards as previously shown on day 1, however on day 2, ChR2 rats center of mass significantly shifts forward. Two-way ANOVA, Dunnett post hoc: ChR2- day 1 vs ChR2+ day 2 p=0.0032; ChR2+ day 1 vs ChR2+ day 2 p=0.0033; ChR2- day 2 vs. ChR2+ day 2 p=0.039. *p<0.05.

(C) Average place field size on the altered task.

(D) Average place field size on the familiar task. Kruskal-Wallis, Dunn post hoc: ChR2- day 1 vs ChR2+ day 2 p=0.045, ChR2- day 2 vs ChR2+ day 2 p=0.027. Data displayed as mean ± sem.

A

Change in Spindle Occurence
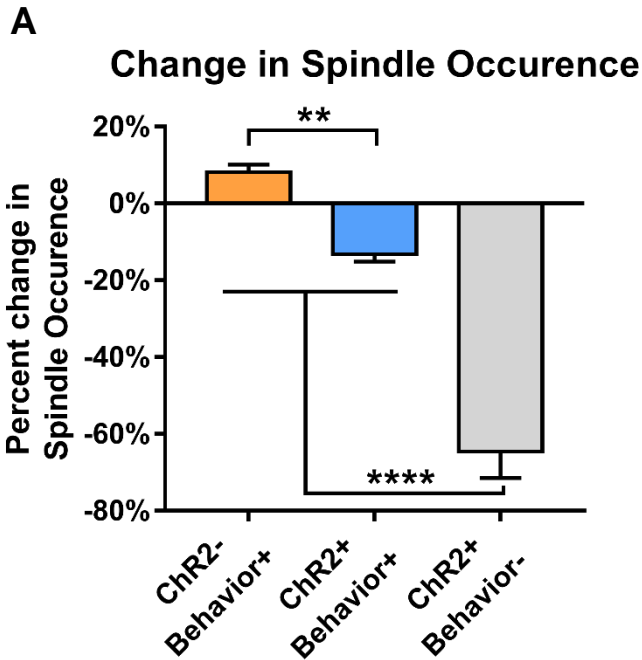
Figure S4. Training mitigates the detrimental effects of LC stimulation on spindle occurrence. Related to Figure 6

(A) The effect of LC stimulation on spindle occurrence in rats performing the behavioral task (Behavior+) vs rats undergoing stimulation in the absence of behavior (Behavior-). Training on a spatial maze task reduces the effect of LC stimulation on spindle occurrence reduction. One-way ANOVA, Tukey post hoc: ChR2-Behavior+ vs ChR2+Behavior+ p=0.008; ChR2-Behavior+ vs ChR2+Behavior- p<0.0001; ChR2+Behavior+ vs ChR2+Bhavior- p<0.0001. **p<0.01, ****p<0.0001. ChR2-Behavior+ n=5, ChR2+Behavior+ n=4, ChR2+Behavior- n=4. Data displayed as mean ± sem.
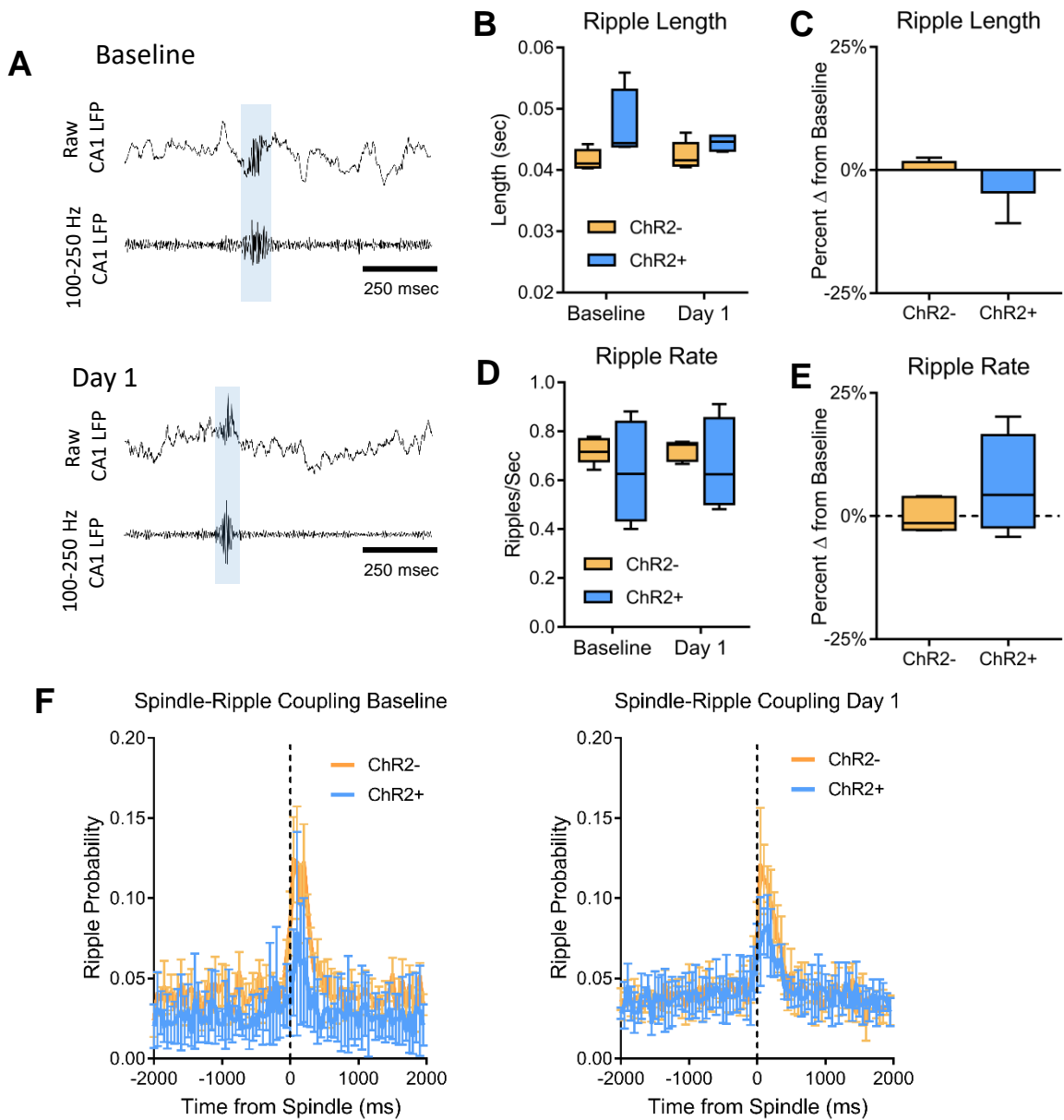
Figure S5. LC stimulation during sleep has no effect on ripple occurrence or length. Related to Figure 7

(A) Representative automatically identified ripple during baseline NREM sleep, and during Day 1 NREM sleep with LC stimulation from ChR2+ rat.

(B) NREM sleep ripple occurrence rate during baseline and day 1 sleep.

(C) Percent change in NREM sleep ripple occurrence rate between baseline sleep and day 1 sleep with LC stimulation.

(D) NREM sleep ripple occurrence rate between baseline and day 1 sleep.

(E) Percent change in NREM sleep ripple rate between baseline sleep and day 1 sleep with LC stimulation.

Box and whisker plots: box displays first and third quartile with median, whiskers display maximum and minimum values. Five ChR2- rats, four ChR2+ rats for part B-E. Bar graph displays mean ± sem.

(F) The probability of a ripple occurring in relation to the onset of a spindle during baseline sleep (left) and during day 1 sleep (right). Displayed as mean probability ± sem.

	n	Spindle Occurrence Percent Change		REM theta power Percent Change		Spindle-Ripple Coupling Change		Ripple Occurrence Percent Change		NREM-SWS Delta Power Percent Change	
		rho	p value	rho	p value	rho	p value	rho	p value	rho	p value
Familiar Task	9	-0.8	**0.014***	-0.67	0.055	-0.79	**0.014***	0.24	0.53	-0.30	0.43
Familiar Task ChR2- Only	5	-0.15	0.83	0.2	0.91	-0.67	0.26	0.10	0.90	0.10	0.90
Familiar Task ChR2+ Only	4	-0.2	0.92	0.41	0.50	0.8	0.33	0.01	0.99	0.4	0.75
Altered Task	9	-0.72	**0.032***	-0.72	**0.034***	-0.83	**0.008***	0.23	0.54	-0.35	0.35
Altered Task ChR2- Only	5	-0.05	0.99	-0.4	0.75	-0.67	0.27	0.36	0.57	0.01	0.99
Altered Task ChR2+ Only	4	0.40	0.75	0.41	0.50	0.4	0.75	-0.40	0.75	0.21	0.73
Familiar Task P-Errors	9	-0.57	0.11	-0.88	**0.0032****	-0.75	**0.023***	0.18	0.65	-0.73	**0.032***
Familiar Task P-Errors ChR2- Only	5	0.72	0.17	-0.56	0.43	-0.10	0.90	-0.36	0.63	-0.82	0.133
Familiar Task P-Errors ChR2+ Only	4	0.80	0.33	-0.40	0.75	0.20	0.92	-0.20	0.92	-0.6	0.42
Familiar Task M- Errors	9	-0.84	**0.0078***	-0.41	0.27	-0.8	**0.013***	0.16	0.67	0.034	0.94
Familiar Task M-Errors ChR2- Only	5	-0.36	0.63	0.67	0.27	-0.56	0.37	0.46	0.43	0.74	0.33
Familiar Task M-Errors ChR2+ Only	4	-0.74	0.33	0.63	0.50	-0.32	0.67	-0.11	0.99	0.41	0.50
Altered Task P-Errors	9	-0.63	0.08	-0.84	**0.0057****	-0.7	**0.042***	0.14	0.71	-0.75	**0.025***
Altered Task P-Errors ChR2- Only	5	0.37	0.53	-0.37	0.53	0.26	0.67	-0.53	0.47	-0.95	0.07
Altered Task P-Errors ChR2+ Only	4	0.80	0.33	-0.40	0.75	0.20	0.92	-0.20	0.92	-0.6	0.42
Altered Task M-Errors	9	-0.64	0.07	-0.23	-0.21	-0.59	0.13	0.24	0.53	0.15	0.70
Altered Task M-Errors ChR2- Only	5	-0.2	0.78	0.60	0.5	0.45	0.23	0.10	0.90	0.3	0.68
Altered Task M-Errors ChR2+ Only	4	-0.95	0.17	0.21	0.83	0.11	0.99	0.01	0.99	0.74	0.33

Table S1. Correlation Table of Day 5 behavioral vs changes from baseline sleep to day 1 sleep. Related to Figure 6
Correlations of day 5 task performance with changes in spindle occurrence, REM theta, spindle-ripple coupling, and ripple occurrence, and NREM sleep delta power. All correlations were performed using Spearman's rho which is displayed above with its p-value. Significant correlations are in bold: *p<0.05, **p<0.005. M-Errors = Map Errors, P-Errors = Procedural Errors